ISSN 0869-5911, Petrology, 2018, Vol. 26, No. 6, pp. 599–616. © Pleiades Publishing, Ltd., 2018.
Original Russian Text © A.L. Perchuk, V.O. Yapaskurt, N.G. Zinovieva, M.Yu. Shur, 2018, published in Petrologiya, 2018, Vol. 26, No. 6, pp. 612–632.

Experimental Evidence for Opposite Fluxes of Sodium, Potassium, and CO_2 during Glaucophane Schist Interaction with Harzburgite and Websterite in Subduction Zones

A. L. Perchuk[a, b, *], V. O. Yapaskurt[a], N. G. Zinovieva[a], and M. Yu. Shur[a]

[a] *Faculty of Geology, Moscow State University, Moscow, 119234 Russia*
[b] *Korzhinsky Institute of Experimental Mineralogy, Russian Academy of Sciences, Chernogolovka, Moscow oblast, 142432 Russia*
**e-mail: alp@geol.msu.ru*

Received April 2, 2018; in final form, May 31, 2018

Abstract—This paper reports the results of high-pressure experimental modeling of interaction between glaucophane schist and harzburgite or websterite for the evaluation of the influence of mantle material on the input–output of components and character of metasomatic transformations at the crust–mantle boundary in the subduction zone. In all experiments, glaucophane schist (proxy for oceanic crust) containing volatile components (H_2O and CO_2) incorporated in hydrous minerals (amphiboles, phengite, and epidote) and calcite was loaded into the bottom of each capsule and overlain by mantle material. During the experiments at a temperature of 800°C and a pressure of 2.9 GPa, which correspond to the conditions of a hot subduction zone, the schist underwent partial (up to 10%) eclogitization with the formation of the anhydrous assemblage omphacite + garnet + quartz ± magnesite ± potassic phase. Carbonate and a potassic phase were formed only in the experiments with websterite in the upper layer. A reaction zone was formed at the base of the websterite layer, where newly formed omphacite, quartz, and orthopyroxene replaced in part initial pyroxenes. Orthopyroxene and phlogopite (or an unidentified potassic phase) were formed in the reaction zone at the base of the harzburgite layer; among the initial minerals, only orthopyroxene relicts were preserved. Above the reaction zones produced by diffusion metasomatism, new phases developed locally, mainly at grain boundaries: newly formed orthopyroxene and magnesite were observed in harzburgite, and omphacite and quartz, in websterite. Alterations along grain boundaries extended much further than the reaction zones, which indicates that fluid infiltration dominated over diffusion in the experiments. The experiments demonstrated that the H_2O–CO_2 fluid with dissolved major components released from the glaucophane schist can produce mineral assemblages of different chemical compositions in mantle materials: Na-bearing in websterite and K-bearing in harzburgite. The complementary components, K_2O and CO_2 for the websterite layer and Na_2O for the harzburgite layer, are fixed in the initial glaucophane schist layer. The distinguished separation of alkalis and CO_2 at the crust–mantle boundary can affect the character of metasomatism in the mantle wedge, primary magma compositions, and the chemical evolution of the rocks of the subducting slab.

Keywords: subduction, mantle, metasomatism, fluid, harzburgite, websterite
DOI: 10.1134/S086959111806005X

INTRODUCTION

Subduction zones are regions where metasomatic transformations of tremendous scale and range of *P–T* conditions occur in mantle wedge rocks under the influence of mobile phase (fluid, melt, or supercritical liquid) flows (Hermann et al., 2006), the main source of which are descending oceanic plates (Schmidt and Poli, 2014; Zheng et al., 2016). The considerable extent of metasomatic processes at the boundary of the subducting plate and overlying mantle results from the contrasting chemical compositions, temperatures, and oxygen fugacities, as well as the amount of fluid (Bebout, 2007). The geochemistry of rocks from subduction zones (volcanics, ultramafics, and high-pressure metamorphics) and data on mineral solubility in fluids allow distinguishing slab components transported by fluids into the overlying mantle. Among them are major elements (Si, Al, Na, K, and Ca); trace elements, including large ion lithophile elements (LILE), light rare earth elements (LREE), U, Th, and Sr; and major volatile components (H_2O, CO_2, and Cl) (Scambelluri and Philippot, 2001; Spandler and Pirard, 2013).

The experimental investigation of mantle metasomatism caused by subduction-related slab components began in the 1980s and has been intensified in the recent years. The *P–T* conditions of these experiments corresponded usually to the crust–mantle

boundary in sub-arc and back-arc parts of subduction zones. Various materials were used as analogues for the suprasubduction mantle, including olivine (Rapp et al., 1999; Perchuk and Yapaskurt, 2013; Grant et al., 2016; Pirard and Hermann, 2015a, 2015b; Perchuk et al., 2018) and, less frequently, altered dunite (Sekine and Wyllie, 1982) and mineral or oxide mixtures corresponding to harzburgite (Bulatov et al., 2014; Woodland et al., 2018), lherzolite (Perchuk et al., 2018), and fertile peridotite (Gervasoni et al., 2017). Metasomatic agents were represented by either various "melts": granite, siliceous glass, carbonate, and carbonate–silicate material (Sekine and Wyllie, 1982; Pirard and Hermann, 2015a, 2015b; Gervasoni et al., 2017) or fluids (produced by decomposition of H_2O- and CO_2-bearing minerals) and melts (produced by partial melting) generated directly in experiments with various crustal analogues, including altered basalt (Rapp et al., 1999), amphibolite (Khodorevskaya and Zharikov, 1997; Perchuk et al., 2013), glaucophane schist (Perchuk and Yapaskurt, 2013; Perchuk et al., 2013), plagioclase (Grant et al., 2016), and synthetic mixtures corresponding in composition to subducted sediments (Bulatov et al., 2014; Woodland et al., 2018) and eclogite (Gervasoni et al., 2017). Since most of the aforementioned experiments were conducted with a single mantle material and a single metasomatic agent, the influence of the lithology of mantle rocks on the character of metasomatic transformations and the composition of residual fluid remains unknown. In this paper, we present the results of a direct comparison of metasomatism in two mantle rock analogues, harzburgite and websterite, caused by fluid derived from carbonate-bearing glaucophane schist under identical *P–T* conditions and run durations.

METHODS

Starting Materials

Glaucophane schists are products of the high-pressure metamorphism of basic rocks of subducting oceanic crust. Recent thermomechanical modeling of subduction zones (van Keken et al., 2011) suggested that glaucophane schists are the most common protoliths of eclogites. Therefore, a fresh glaucophane schist sample from the Atbashi high-pressure complex in Kyrgyzstan (collection of N.G. Udovkina) was used as a model analogue for the subducting crust. The foliation of the rock is cut by numerous thin (5–100 μm thick) veinlets filled with winchite, phengite, epidote, chlorite, calcite, and albite. In the first experimental series (hereafter, series 1), we used a powder of glaucophane schist consisting of more than 95% amphiboles, winchite and glaucophane, the latter being much more abundant. The petrographic characteristics of the sample and mineral proportions in the powder used in series 1 experiments were reported by Perchuk and Yapaskurt (2013) and Perchuk et al. (2013). In order to confirm and refine the obtained results, an additional experimental series (hereafter, series 2) was conducted under the same *P–T* conditions and run durations, but using newly prepared starting materials. In particular, a new batch was made from the same glaucophane schist sample (AT97) for series 2, because the initial powder was exhausted. The ultramafic mixtures were also modified (see below).

Data on mantle xenoliths from the volcanics of Pacific subduction zones (Arai and Ishimaru, 2008) indicate that, despite considerable lateral variations and difference between samples from different subduction zones, harzburgite is the most abundant mantle-wedge rock. Dunites and lherzolites are also rather common, whereas pyroxenites are rarer, although their fraction is significant in some subduction zones (Arai and Ishimaru, 2008; Figs. 3b, 3c). It was noted above that olivine and, less frequently, a mixture of olivine, clinopyroxene, and orthopyroxene were used in our experiments. In this study, we used mixtures of monomineralic separates corresponding in mineral proportions to harzburgite and websterite (Table 1).[1] The harzburgite mixture for series 1 experiments consisted of equal mass fractions of olivine and orthopyroxene, and the websterite mixture consisted of orthopyroxene and clinopyroxene in a 2 : 1 proportion. The mixtures for these experiments were prepared using olivine from Aheim dunite, Norway, and pyroxenes from pyroxenite veins in the Voikar ophiolite complex, Polar Urals (kindly provided by G.N. Savelyeva). Similar to our previous experiments (Perchuk et al., 2018), olivine, orthopyroxene, and clinopyroxene fractions from a lherzolite nodule in alkali basalt of Victoria, Australia (kindly provided by O.G. Safonov) were used in series 2. The harzburgite (olivine + orthopyroxene) and websterite (clinopyroxene + orthopyroxene) mixtures were prepared from equal mass fractions of minerals.

The compositions of minerals used as starting materials are given in Table 1.

Experimental Methods

Starting mixtures for series 1 were ground to a grain size of 5–80 μm and loaded into 5 mm long platinum capsules with an outer diameter of 3 mm; a glaucophane schist layer was overlain by a layer of mantle material (websterite or harzburgite) of approximately the same volume. Such a sample configuration corresponded in general to the relative position of crustal and mantle rocks in the sub-arc region of subduction zones, where subduction channels with tectonic mélange pinch out (Cloos, 1992; Gerya et al., 2002), and provided upward migration of fluid (melt) released from the schist through the whole capsule. Similar to our previous experiments (e.g., Perchuk et al., 2013), the capsule was welded only at the lower end,

[1] The names of respective rocks, websterite and harzburgite, were used for the mixtures.

Table 1. Microprobe analyses of starting minerals and the chemical composition of glaucophane schist, wt %

	Glaucophane schist				Ultramafic rocks, series 1			Ultramafic rocks, series 2		
Component	Bulk*	*Gln*	*Win*	*Phn*	*Cpx*	*Ol*	*Opx*	*Cpx*	*Ol*	*Opx*
SiO_2	55.12	55.29	55.14	49.88	54.04	40.17	56.74	51.91	40.36	54.83
TiO_2	0.54	0.19	0.01	0.38	0.08	0	0.00	0.10	0	0.03
Al_2O_3	10.73	10.13	1.47	26.07	1.08	0.08	0.36	5.24	0.17	3.66
Cr_2O_3	0.02	0.02	0.01	0.22	0.60	0.01	0.10	1.08	0.01	0.46
FeO	12.27**	12.60	13.08	2.16	2.63	6.80	8.73	2.47	8.69	5.66
MnO	0.07	0.32	0.19	0.11	0.13	0.13	0.18	0.03	0.12	0.08
MgO	10.72	9.48	16.05	4.36	17.57	51.78	33.53	15.68	49.13	33.63
CaO	2.33	2.13	9.65	0.09	23.25	0.0	0.57	20.41	0.05	0.70
Na_2O	6.16	6.41	2.02	0.42	0.53	0.0	0.0	1.54	0.21	0.21
K_2O	0.16	0.07	0.02	11.03	0.04	0.0	0	0.02	0.02	0
NiO	0.03	b.d.l.	b.d.l.	b.d.l.	0.08	0.37	0.07	0.10	0.37	0.10
Total	98.15	96.64	97.63	94.7	100.01	99.94	100.47	98.39	99.07	99.54
$Mg/(Mg + Fe^{2+})$		0.72	0.79	0.78	0.92	0.93	0.87	0.92	0.91	0.91

* XRF analysis of glaucophane schist used in series 1 (analyst A.I. Yakushev, Institute of Geology of Ore Deposits, Petrography, Mineralogy, and Geochemistry, Russian Academy of Sciences). LOI = 1.75 wt %. ** Fe_2O_3.

and the upper lid was tightly fitted by bent wall edges (with overlap). The incomplete sealing of the capsule at the side of mantle material bears some similarity to natural conditions in that part of fluid penetrating through the mantle material could leave the system. The capsule was inserted in the center of a high-pressure salt cell, which was described by Perchuk et al. (2013).

In the series 2 experiments, starting materials were ground to a smaller grain size of 5–10 μm and loaded into 4 mm long $Ag_{30}Pd_{70}$ capsules with an outer diameter of 2 mm. The experiments of this series were conducted in hermetically sealed capsules, similar to the overwhelming majority of experiments in the aforementioned studies of subduction processes. The isolation of material in these experiments was additionally improved by the use of $Ag_{30}Pd_{70}$, which does not absorb iron in contrast to platinum capsules employed in series 1. Each capsule was placed into the high-pressure cell in the zone of a minor temperature gradient (5°C/mm), which enhanced the migration of components in the fluid flow (Rapp et al., 1999; Perchuk et al., 2018; Woodland et al., 2018). The configuration of the cell was described by Perchuk et al. (2018).

Experiments were conducted in a piston–cylinder apparatus at the Institute of Experimental Mineralogy of the Russian Academy of Sciences at a temperature of 800°C and a pressure of 2.9 GPa, which corresponds to hot subduction zone geotherms at the crust–mantle boundary estimated by thermomechanical modeling (Syracuse et al., 2010). The pressure calibration of the apparatus was reported by Perchuk et al. (2013). Oxygen fugacity was not controlled during experiments. According to Patiño Douce and Harris (1998), cell assemblies with graphite heaters maintain $\log f O_2$ values between the fayalite–magnetite–quartz (FMQ) buffer and FMQ-2, which corresponds to conditions estimated for suprasubduction mantle peridotite (Foley, 2011). The run duration was approximately three days (Table 2). Temperature was measured by a WRe5/20 thermocouple at the upper end of the capsule. The main parameters of experiments are given in Table 2.

After the experiment, the capsule was mounted in polystyrene, sectioned lengthwise, and polished using diamond pastes.

Analytical Methods

The electron microscope examination and electron microprobe analysis of the starting phases and experimental products were conducted at the Laboratory of Analytical Techniques of High Spatial Resolution of the Petrology Department of the Geological Faculty, Moscow State University.

The products of series 1 experiments were investigated on a Jeol JSM-6480LV electron microscope with an Inca Energy-350 energy dispersive system and at the Institute of Experimental Mineralogy, Russian Academy of Sciences on a Tescan Vega II XMU scanning electron microscope with an Inca Energy-450 energy dispersive system. Back-scattered electron images were obtained at an accelerating voltage of 20 kV, and quantitative energy dispersive analysis was conducted at an accelerating voltage of 20 kV and a beam current of 0.7 nA.

Table 2. Run conditions and products at $T = 800°C$ and $P = 2.9$ GPa

Run	Duration, h	Capsule	Starting materials*		Run products**			Comment
			lower layer*	upper layer	lower layer (Gls)	reaction zone (RZ)	upper layer (Wbs or Hz)	
Sub40	72	Pt	Gls	Wbs1	*Omp, Grt, Opx*$_3$, *Qz, Bt*, (Gl)	*Omp, Qz, Opx*$_2$, (*Cpx*$_{ini}$, *Opx*$_{ini}$)	*Omp, Qz,* (*Opx*$_{ini}$, *Cpx*$_{ini}$)	Series 1, non-hermetic capsule
Sub41	67	Pt	Gls	Hz	*Omp, Grt,* ± *Qz,* (Gl)	*Opx*$_2$, *Phl,* (*Opx*$_{ini}$)	*Opx*$_2$, *Mgs, Chl,* (*Ol*$_{ini}$, *Opx*$_{ini}$)	Series 1, non-hermetic capsule
Sub111	72	$Ag_{30}Pd_{70}$	Gls	Wbs2	*Omp, Grt, Qz,* Fe-Mg carb, *K-phase*, (Gl)	*Omp, Qz, Opx*$_2$, (*Cpx*$_{ini}$, *Opx*$_{ini}$)	*Omp, Qz,* (*Opx*$_{ini}$, *Cpx*$_{ini}$)	Series 2, hermetic capsule
Sub113	72	$Ag_{30}Pd_{70}$	Gls	Hz	*Omp, Grt,* ± *Qz,* (Gl)	*Opx*$_2$, K-phase (*Opx*$_{ini}$)	*Opx*$_2$, *Mgs,* (*Ol*$_{ini}$, *Opx*$_{ini}$)	Series 2, hermetic capsule

* Abbreviations for starting materials: Gls, natural glaucophane schist; Hz, model harzburgite (*Ol–Opx* mixture in 1 : 1 weight proportion); Wbs1, model websterite (*Cpx–Opx* mixture in 1 : 2 weight proportion); Wbs2, model websterite (*Cpx–Opx* mixture in 1 : 2 weight proportion). **Mineral and melt symbols: *Omp*, omphacite; *Grt*, garnet; *Am,* amphibole; *Qz*, quartz; *Chl,* chlorite; *Fe–Mg carb*, Fe–Mg carbonate (breunnerite); *Mgs*, magnesite; *Opx,* newly formed orthopyroxene; *Phl,* phlogopite; *Bt,* biotite (see text for details of compositions); *K-phase*, potassic phase; L, presumed melt. Mineral symbols in parentheses are relicts of initial phases (e.g., *Cpx*$_{ini}$).

The products of series 2 experiments were investigated on a Superprobe JXA-8230 electron microprobe with a tungsten thermal emission cathode. Back-scattered electron images were obtained at an accelerating voltage of 20 kV. The quantitative wavelength-dispersive analysis of all minerals, except for carbonates, was conducted with a focused electron beam at an accelerating voltage of 20 kV and a beam current of 20 nA. Natural silicates were used as standards for major elements. The counting time for major elements was 30 s for the peak and 15 s for the background. Under such conditions, the variance of the measurement of major elements was no higher than 0.9% relative.

The spatial distribution of products of fluid–mineral reactions in the capsule and their quantitative relations were evaluated using maps of the distribution of chemical elements constructed on the basis of intensities of characteristic X-rays at an accelerating voltage of 20 kV and a beam current of 40 nA. The mapping was carried out with a step size of 1 μm on the basis of 10 passes at a counting time of 10 ms at each spot.

The character of changes in bulk chemical composition in the contact zone between glaucophane schist and websterite in the series 1 experiments was explored by the method of integrated profiles described by Perchuk et al. (2013).

RUN PRODUCTS

The products of both series reflect similar metasomatic processes. However, there are some minor but important differences in mineral composition related probably to different contents of carbonate in the glaucophane schist mixtures (Table 2). Newly formed phases can be observed both within the initial materials and at the boundary zone between them, which is referred to as the reaction zone (Figs. 1, 2). The products of run Sub41 (series 1) were described briefly by Perchuk et al. (2013), and here we present a more detailed report.

The structures of glaucophane schist layers in the products of series 1 experiments are similar. They are composed of more than 80% of relatively large grains of starting glaucophane, and an aggregate of small (up to 5 μm) omphacite grains and rare quartz and euhedral garnet crystals develops along the boundaries between glaucophane grains (Figs. 1c, 1f). In run Sub40, orthopyroxene occurs sporadically near the contact with websterite, and rare aggregates of biotite flakes were observed at the base of the glaucophane schist layer (Fig. 3a). Remember that the presence of a potassic phase was confirmed in a similar experiment of series 2 with pure materials (Table 2). It is interesting that potassic phases are missing in the modified glaucophane schist layer from run Sub41. In previous experiments conducted on the same apparatus under identical $P–T$ conditions, quartz was identified by Raman spectroscopy (Perchuk et al., 2018), which is consistent with its stability field (Bose and Ganguly, 1995). This allows us to suggest that quartz rather than coesite was probably formed in the experiments described here.

In the series 2 experiments, the development of omphacite aggregates is less pronounced (Figs. 2c, 2f) compared with series 1 (Figs. 1c, 1f). Nonetheless, there are numerous subhedral garnet crystals at the boundaries of omphacite grains (Fig. 2). In the glaucophane schist layer of run Sub111, extensive magnesite crystallization was observed (Fig. 2f). A potassic

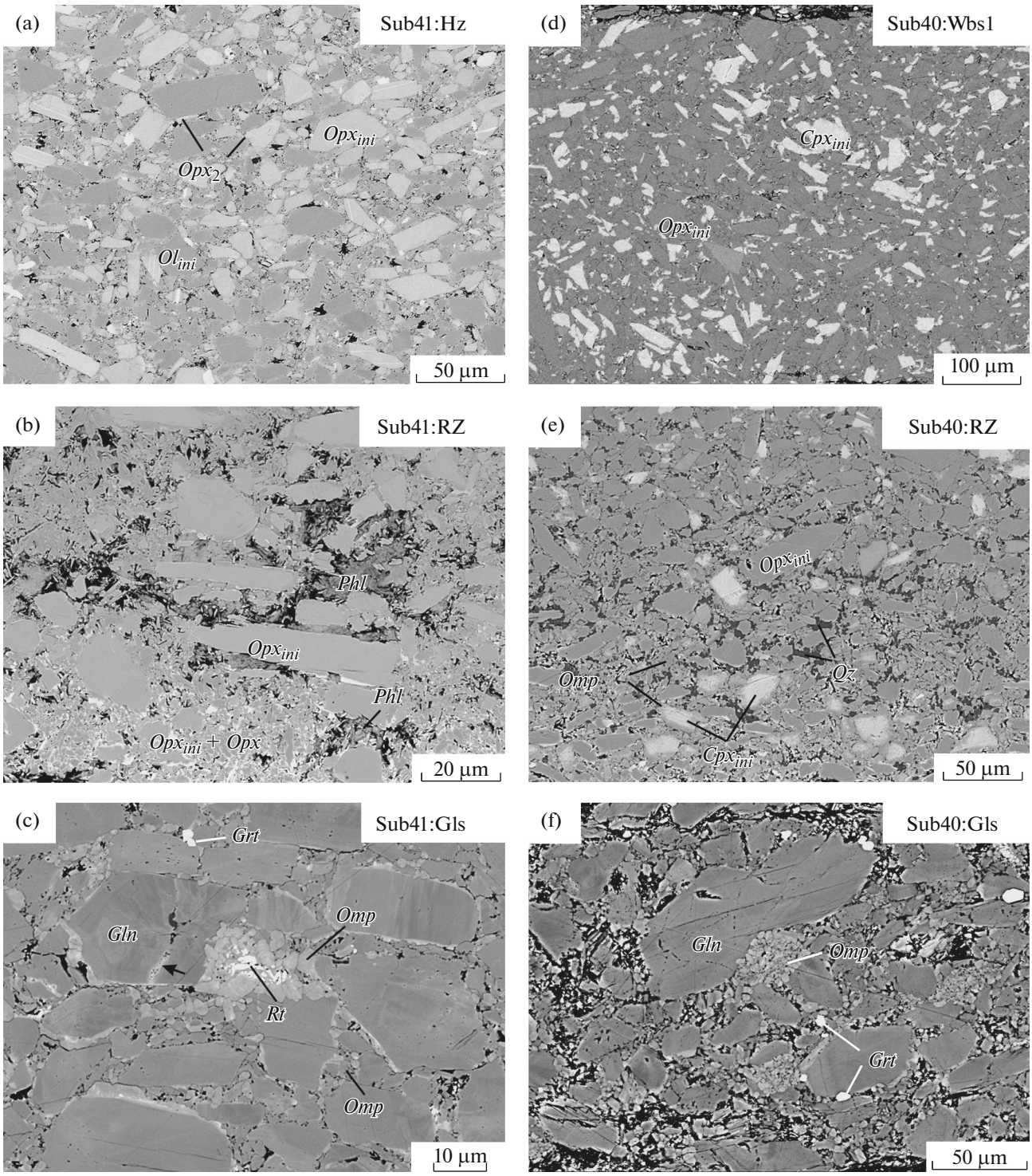

Fig. 1. Back-scattered electron images of representative areas of the main zones of the products of series 1 experiments in the systems glaucophane schist (Gls)–websterite (Wbs) (Sub40) and glaucophane schist (Gls)–harzburgite (Hz) (Sub41). (a) Hz layer from run Sub41, (b) reaction zone from run Sub41, (c) Gls layer from run Sub41, (d) Wbs layer from run Sub40, (e) reaction zone from run Sub40, and (f) Gls layer from run Sub40.

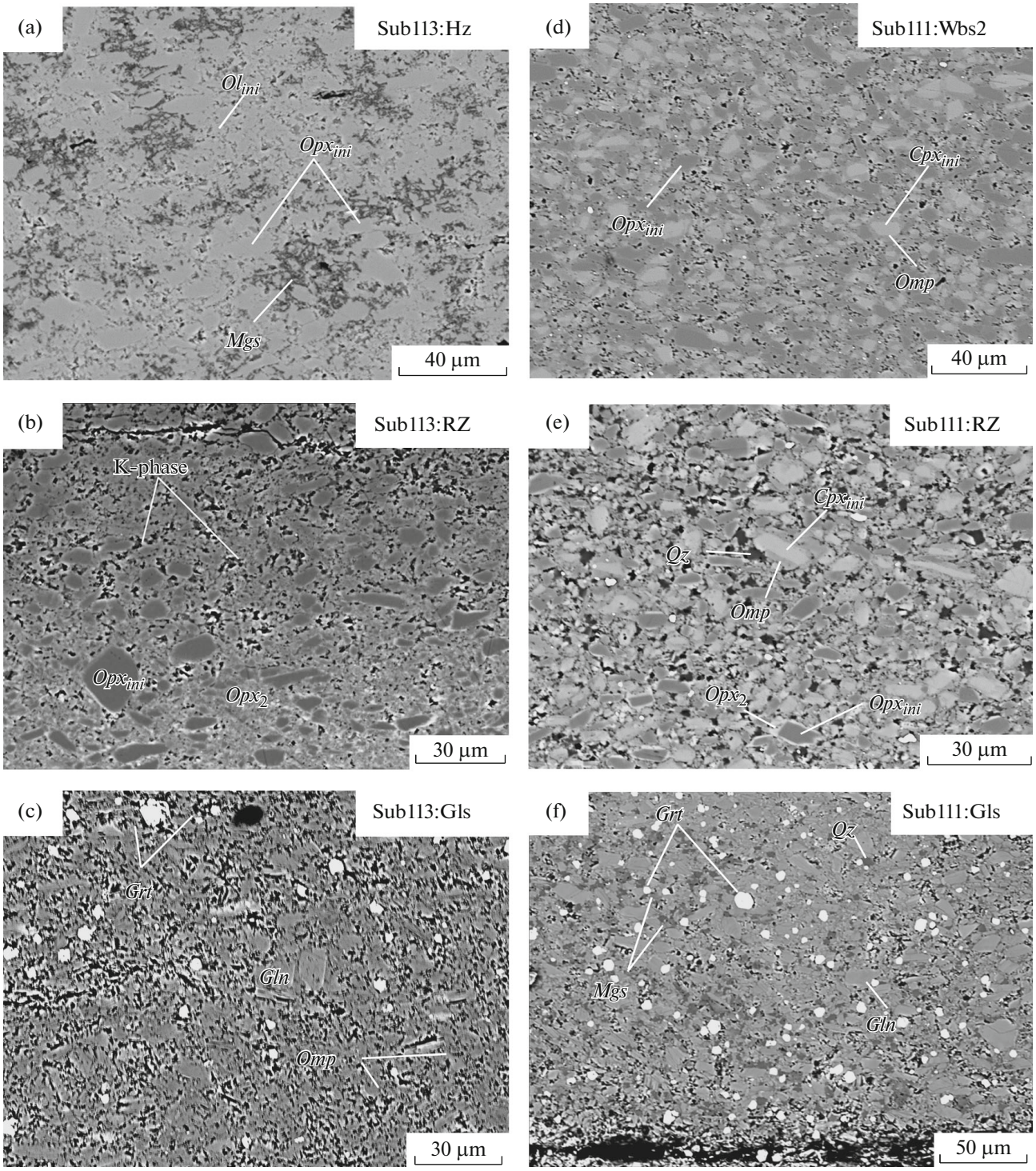

Fig. 2. Back-scattered electron images of representative areas of the main zones in the products of series 2 experiments in the systems glaucophane schist (Gls)–websterite (Wbs) (Sub111) and glaucophane schist (Gls)–harzburgite (Hz) (Sub113). (a) Hz layer from run Sub113, (b) reaction zone from run Sub113, (c) Gls layer from run Sub113, (d) Wbs layer from run Sub111, (e) reaction zone from run Sub111, and (f) Gls layer from run Sub111.

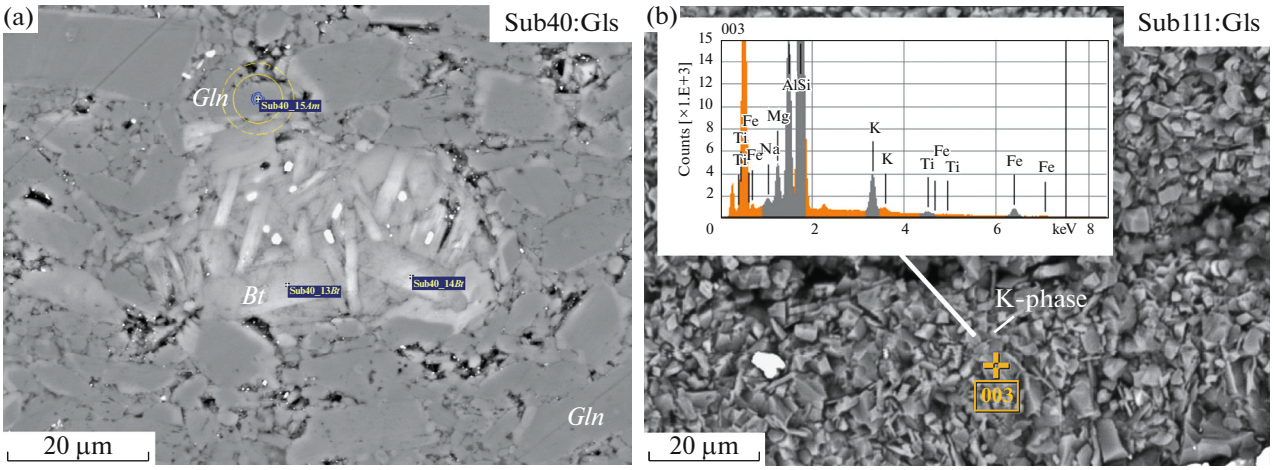

Fig. 3. Back-scattered electron images of potassic phases at the base of the glaucophane schist layers in the products of runs (a) Sub40 and (b) Sub111. The inset in Fig. 3b shows the energy-dispersive spectrum of the potassic phase at the indicated spot (no. 003). Comments to microprobe analyses conducted in an automatic mode (run number, analysis number, and mineral symbol) are shown in blue rectangles. The cross indicates the spot of microprobe analysis.

phase appears in the lower part of this layer, but it was too small for identification (Fig. 3b). Similar to run Sub41 of series 1, no potassic phase was found in the glaucophane schist layer of run Sub113.

Thus, potassic phases were formed in the lower layer only in the experiments with the websteritic upper layer.

The mineral composition of reaction zones is consistently reproduced in both run series and is controlled mainly by the mantle material (Figs. 1b, 1e; Table 2). The reaction zone after harzburgite contains relicts of initial orthopyroxene cemented by tabular and acicular crystals of newly formed orthopyroxene and phlogopite flakes in series 1 (Fig. 1b) or tiny grains of an unidentified potassic phase in series 2 (Fig. 2b). It is clearly seen in back-scattered electron images that newly formed iron-rich orthopyroxene often occurs as thin rims around the initial orthopyroxene (Figs. 1b, 2b). The distribution of minerals in the transition zone and their modal contents are shown in the phase map of run Sub41 (Fig. 4a). Olivine was not detected in the reaction zones.

Quartz, omphacite, and newly formed orthopyroxene rimming initial orthopyroxene grains occur in the reaction zone at the base of the websterite layer (Figs. 1f, 2f). Relicts of initial clinopyroxene are often preserved in the cores of omphacite. The phase map of run Sub40 exhibits a significant increase in the volume fraction of clinopyroxene (omphacite and relict clinopyroxene) compared with the starting mixture (Fig. 4b).

It is evident that the mineralogical characteristics of reaction zones developing in different materials are significantly different, which results in the retention of different alkali components: potassium in harzburgite (Fig. 5) and sodium in websterite (Fig. 6).

Changes in the websterite layer above the reaction zone were very similar in the two series. Omphacite rims developed around clinopyroxene, and submicrometer quartz grains appeared along grain boundaries. The extent of transformation in run Sub111 is much higher than that in run Sub40. Orthopyroxene and magnesite were formed in the harzburgite layer. Very thin chains (a few micrometer or less than one micrometer across) of orthopyroxene and presumably submicrometer magnesite were observed in run Sub41. A similar replacement is much more extensive in run Sub113. For instance, the modal content of magnesite is up to 10%. A few chlorite grains were found in the lower part of the layer in run Sub41.

Because of the absence of melt segregation zones or thin melt films, the mobile phase in the experimental products will be referred to as fluid, although the presence of a hydrous melt cannot be excluded.

COMPOSITIONS OF MINERALS

The electron microprobe analyses of the starting minerals are given in Table 1, and those of the newly formed phases, in Tables 3 and 4. Because of the small size of phases, X-ray excitation in neighboring minerals might affect the quality of the analyses.

Garnet always occurs as a newly formed phase. It was observed in all experiments in the middle and upper parts of the glaucophane schist layer. The compositions of garnet in all runs are rather similar: X_{Mg} = 0.28–0.30 and X_{Ca} = 0.09–0.13.

Clinopyroxene occurred as a starting phase in the websterite layer and was formed in all layers and reaction zones during the experiments. The initial clinopyroxene of the websterite layer was augite with X_{Mg} ~ 0.92 and slightly different contents of the jadeite end-mem-

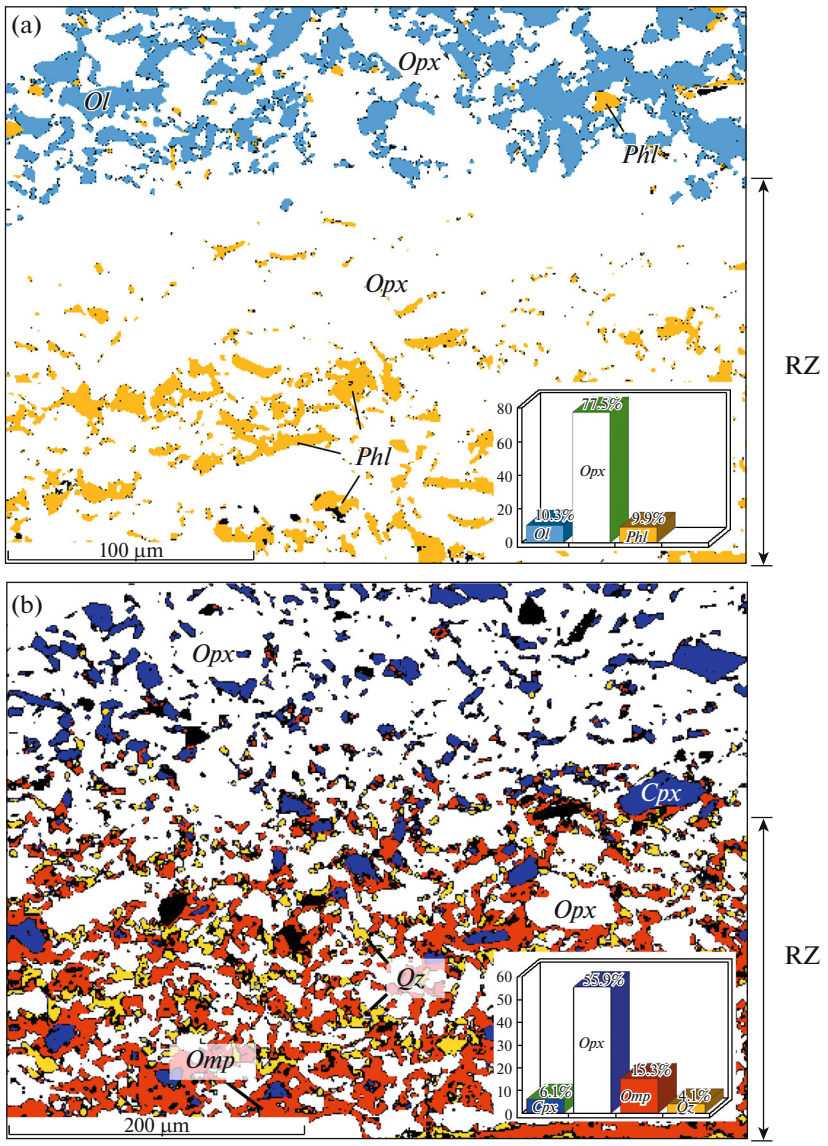

Fig. 4. Phase maps of reaction zones at the base of the layers of mantle materials: (a) harzburgite, run Sub41 and (b) websterite, run Sub40.

ber: X_{Jd} ~ 0.01 in run Sub41 (series 1) and X_{Jd} ~ 0.04 in run Sub111 (series 2). In the reaction zones of both series, it was replaced by omphacite with similar compositions: X_{Mg} = 0.83–0.84 and X_{Jd} ~ 0.36. It is significantly different from the omphacite formed after the glaucophane schist: X_{Mg} = 0.61 and X_{Jd} = 0.45–0.47 in both experimental series. The composition of omphacite from the glaucophane schist layer of run Sub113 could not be precisely determined because of the small grain size.

Orthopyroxene was a component of the ultramafic mixtures. Its initial composition in series 1 was less magnesian and aluminous (X_{Mg} ~ 0.87 and Al_2O_3 < 0.5 wt %) compared with series 2 (X_{Mg} ~ 0.91 and Al_2O_3 < 3.5 wt %). Orthopyroxene growth was most pronounced in the reaction zones and was also observed at the boundaries of olivine grains in the harzburgite layer and in the upper part of the glaucophane schist layer in run Sub40. The precise analysis of newly formed orthopyroxene was hindered by fine grain sizes in some zones. In the reaction zones at the base of the harzburgite layer, there is a distinct increase in the X_{Mg} value of orthopyroxene from ~0.85 to 0.90 toward the harzburgite layer. This is accompanied by an increase in Al_2O_3 content in series 1 and a decrease in Al_2O_3 content in series 2 compared with the initial orthopyroxene composition. Orthopyroxene from the upper part of the glaucophane schist layer shows the lowest X_{Mg} value of ~0.87 at Al_2O_3 ~ 2 wt %.

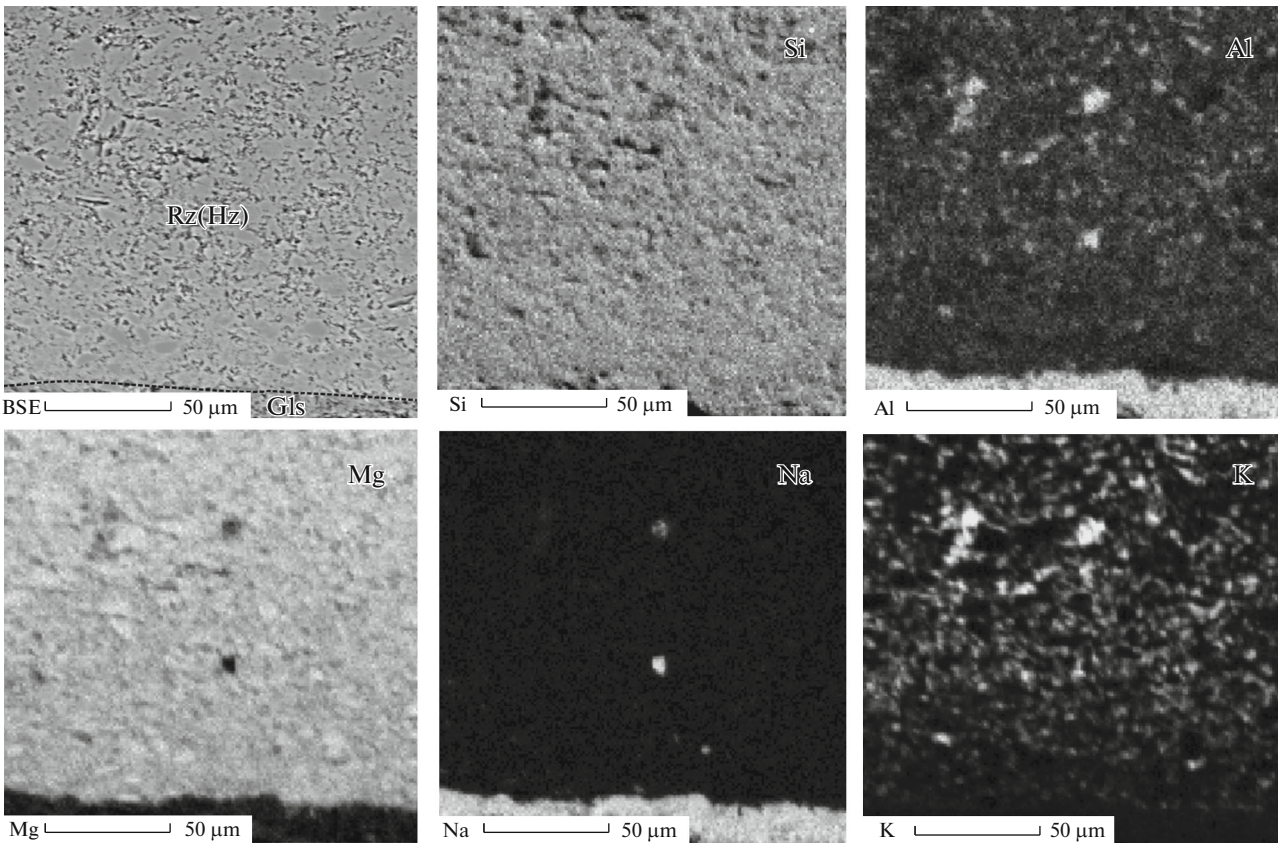

Fig. 5. Back-scattered electron image, Rz(Hz), and element maps of a reaction zone at the base of the harzburgite layer in run Sub113. Note almost complete absence of sodium.

Amphibole in the initial glaucophane schist is mostly glaucophane with a minor amount (<1%) of winchite (according to the classification of Leake et al., 1997).

Micas. The initial glaucophane schist contains a small amount of phengite with a mean Si content of 3.37 atoms per formula unit and $X_{Mg} = 0.77$. The reaction zone of run Sub41 contains phlogopite with elevated Si and low K contents (Fig. 1b, Table 4) indicating the $SiK_{-1}Al_{-1}$ substitution, which is characteristic of ultrahigh-pressure solid solution of phlogopite and talc (Comodi et al., 2011). A phase similar to mica in morphology and spectral characteristics was observed in the reaction zone of run Sub113, but its small size prevented reliable analysis.

Chlorite was found only above the reaction zone in the harzburgite layer of run Sub41. Its composition corresponds to penninite with elevated Cr_2O_3 content (1.42 wt %).

Carbonates. The initial glaucophane schist contains calcite. Instead of calcite, magnesite occurs in the experimental products in the glaucophane schist layer of run Sub111 and the harzburgite layers of runs Sub41 and Sub113. Magnesite from the glaucophane schist layer is less magnesian ($X_{Mg} \sim 0.71–0.75$) than magnesite from the harzburgite layers ($X_{Mg} > 0.91$) (carbonate-free initially).

The starting *olivine* shows constant X_{Mg} values of 0.93 and 0.91 in the series 1 and 2 experiments, respectively.

DISCUSSION

Interpretation of Processes in the Capsules

In the glaucophane schist layer, glaucophane was partly replaced during the experiments by anhydrous minerals (omphacite, garnet, and quartz), which was accompanied by the release of aqueous fluid. The equilibrium character of the process in this layer is supported by the consistent compositions of omphacite and garnet (Table 3) and the results of garnet–clinopyroxene thermometry (Krogh Ravna, 2000): the obtained mean temperature estimate (843°C at 2.9 GPa) appeared to be close to the experimental temperature.

The growth of new minerals in the glaucophane schist layer occurred mainly at the margins of glaucophane grains, which indicates the importance of migrating fluid accelerating mineral reactions and providing component influx and removal. The gener-

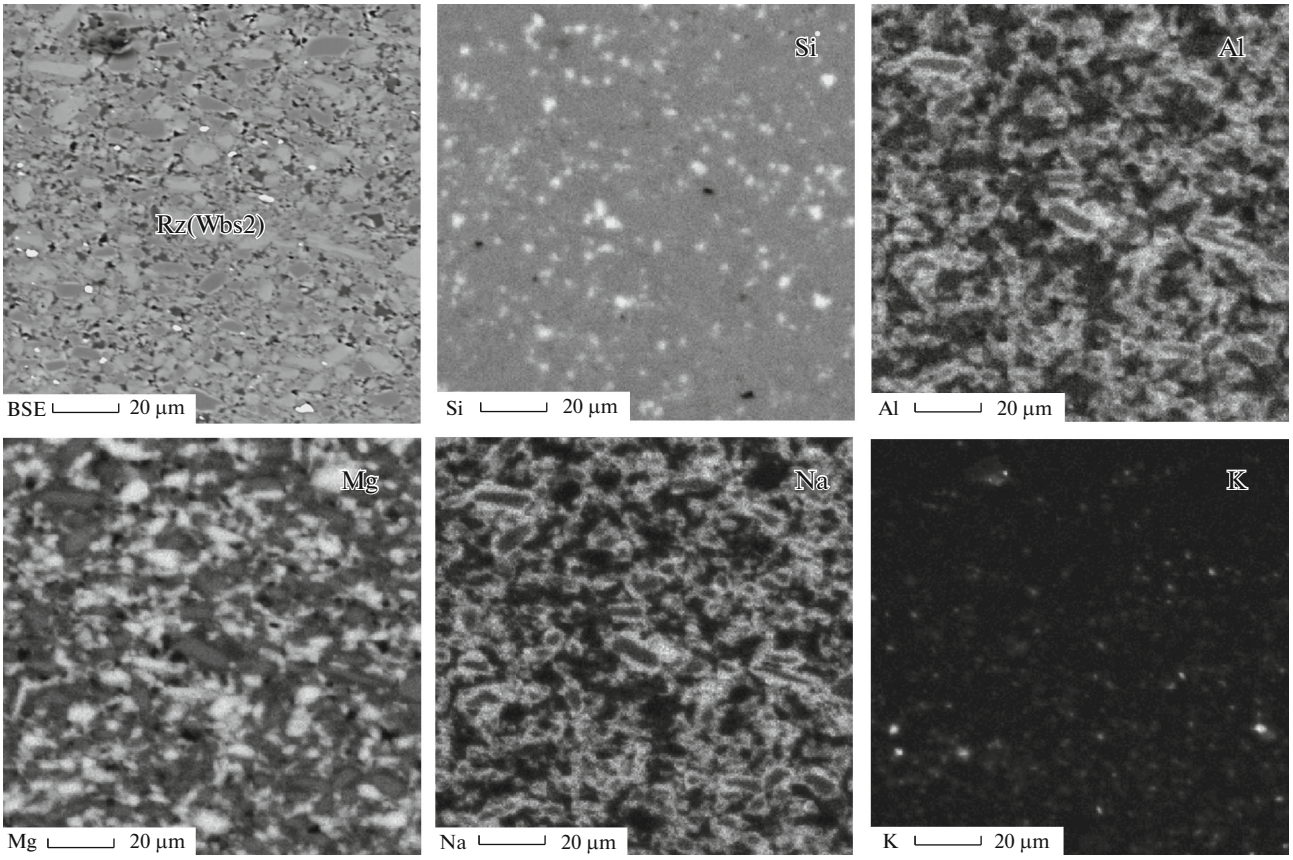

Fig. 6. Back-scattered electron image, Rz(Wbs2), and element maps of a reaction zone at the base of the websterite layer in run Sub111. Note almost complete absence of potassium.

alized scheme of this transformation is the dehydration reaction

$$Am + Phn + Cal \rightarrow Omp + Grt + Qz \pm Mgs \pm K\text{-phase} + H_2O + [SiO_2 + Al_2O_3 + Na_2O + K_2O]_{\text{in fluid}}. \quad (1)$$

In the product of this reaction, magnesite occurs only in run Sub111 (with websterite), and the unidentified K-phase (Sub111) or biotite (Sub40) was obtained in the experiments with harzburgite. Alkalis, aluminum, and silicon are released into the aqueous fluid owing to this reaction. Their presence in the fluid is indicated by the development of new minerals, phlogopite, orthopyroxene, omphacite, and quartz, in and sometimes above the reaction zones (Figs. 1, 2). The formation of these minerals would have been impossible under isochemical conditions because of the deficiency of alkalis and aluminum in the mantle materials.

In the capsules located in the gradient-free zone of the high-pressure cell (series 1), the upward fluid flow into the mantle material was probably driven by the gradient of the chemical potential of H_2O and the gradient of fluid pressure imposed by dehydration reactions. The minor temperature gradient characteristic of series 2 experiments should accelerate fluid migration. This is, perhaps, why the degree of mantle material transformation in series 2 was significantly higher than in series 1. In the experiments of both series, there was no focused fluid flow along capsule walls, which was observed in experiments with amphibolite (e.g., Perchuk et al., 2018). This is probably related to the slow kinetics of recrystallization or specific features of fluid migration through glaucophane schist and, in the series 1 experiments, to the absence of temperature gradient accelerating fluid flow. The existence of a focused flow is clearly manifested by the development of an omphacite–quartz aggregate along the walls in the websterite layer (run Sub111).

Structural and mineralogical observations (Figs. 1, 2) clearly indicate that the fluid generated in the glaucophane schist layer migrated through the whole upper zone. The different metasomatic effects exerted by fluid on a certain material are related to different mechanisms of mass transfer. For instance, the most significant changes in the initial material are observed in the reaction zones, which underwent diffusion metasomatism. In the apoharzburgite reaction zone, olivine replacement by orthopyroxene is accompanied

Table 3. Microprobe analyses of newly formed minerals in the schist layer

Component	Sub40				Sub 41						Sub111				Sub113	
	Grt		*Cpx*		*Grt*		*Cpx*		*Opx*		*Grt*		*Cpx*		*Grt*	
	4*	sd	9	sd	6	sd	3	sd	5	sd	5	sd	7	sd	8	sd
SiO_2	38.2	0.34	54.94	0.27	38.46	0.64	55.67	2.15	51.2	0.50	38.82	0.36	54.73	2.13	38.36	0.43
TiO_2	0.74	0.10	0.48	0.26	0.66	0.13	0.29	0.14	0.05	0.05	0.54	0.08	0.36	0.25	0.50	0.04
Al_2O_3	20.8	0.15	12.42	1.76	21.01	0.44	11.54	0.89	2.14	0.52	21.10	0.23	12.40	0.59	20.96	0.86
Cr_2O_3	0.01	0.01	0.04	0.04	0.03	0.02	0.00	0.00	0.04	0.02	0.02	0.01	0.04	0.03	0.04	0.02
FeO	27.9	0.41	8.47	0.96	28.63	0.82	8.48	0.40	24	0.50	27.79	0.55	8.26	0.60	29.54	0.78
MnO	0.46	0.04	0.13	0.03	0.57	0.19	0.13	0.05	0.15	0.03	0.42	0.04	0.11	0.05	0.49	0.02
MgO	6.62	0.25	7.51	0.85	6.45	0.30	7.23	0.32	19.2	0.55	6.57	0.40	8.18	0.72	6.37	0.40
CaO	4.23	0.33	8.93	1.26	4.17	0.01	9.56	0.98	0.37	0.07	4.84	0.43	7.52	2.48	3.09	0.20
Na_2O	0.02	0.02	7.26	0.73	0.12	0.06	6.72	0.64	0.59	0.14	–		7.02	1.11	–	
K_2O	0.15	0.02	0.02	0.02	0.00	0.01	0.01	0.01	0.00	0.01	–		0.02	0.02	–	
NiO	–		–		–		–		–		–		0.02	0.01	–	
Total	99.15	0.61	100.20	0.46	100.11	1.13	99.63	2.18	97.7	0.82	100.11	0.57	98.63	1.03	99.35	1.00
X_{Mg}	0.30	0.01	0.61	0.02	0.29	0.01	0.62	0.03	0.59	0.01	0.30	0.02	0.64	0.04	0.28	0.02
X_{Ca}	0.12	0.01			0.12	0.00					0.13	0.01			0.09	0.01
X_{Na}^{Bt}																
X_{Jd}			0.46	0.05			0.45	0.05					0.47	0.06		

"sd" is standard deviation, and a dash indicates that the element was not analyzed. * Number of analyses.

by phlogopite growth (Figs. 1b, 2b). The generalized reaction of this process

$$Ol + H_2O + [SiO_2 + Al_2O_3 + K_2O]_{\text{in fluid}} = Opx_2 + Phl + [MgO]_{\text{in fluid}} \quad (2)$$

emphasizes the influx of silicon, potassium, and water. Since the newly formed assemblage is poorer in Mg than olivine, this element had to escape from the reaction zone. The Mg flux is probably directed into the relatively Mg-poor glaucophane schist rather than into the magnesian harzburgite. It is important that Na was not observed either in the reaction zone or in metasomatically affected grain boundaries in the harzburgite layer. It was probably fixed in newly formed omphacite in the glaucophane schist layer.

The growth of quartz and omphacite in the reaction zone of the websterite layer (Figs. 1e, 2e) occurred at the expense of silicon, aluminum, and sodium influx:

$$Cpx_{ini} + [SiO_2 + Al_2O_3 + Na_2O]_{\text{in fluid}} = Omp + Qz + [MgO + CaO]_{\text{in fluid}}. \quad (3)$$

The extensive replacement of augite by omphacite implies Mg and Ca removal from this zone (Fig. 3). These components probably descended into the schist zone along the concentration gradient and contributed to the formation of omphacite and orthopyroxene, which was observed in run Sub40. Potassium, which played an important role in the apoharzburgite reaction zone, was in no way manifested in the websterite layer, including the reaction zone. It cannot be excluded that small amounts of K could be present in submicrometer films of silicic melt (if it existed), but the main K reservoir is the lower part of the glaucophane schist layer, where biotite and an unidentified K phase were observed. It is evident that K migration was not controlled by an initial concentration gradient, because there was no K gradient in the initial schist. Note that the described key phenomena of mass transfer of major components were observed in our experiment with a duration of 190 h at 800°C and 2.9 GPa (Sub59, our unpublished data). In this experiment, a sample consisting of a carbonated amphibolite layer overlain with websterite was loaded into a capsule without an upper lid and placed into the gradient-free zone of the pressure cell. In the run products, K was concentrated in phengite developing at the base of the eclogitized amphibolite layer, an omphacite–quartz–orthopyroxene–magnesite assemblage was observed in the reaction zone, and omphacite and quartz grew along grain boundaries in the upper zone. It can be seen that the only difference from the experiments described in this paper is the character of CO_2 migration. In run Sub59, carbon was transported from the

Table 4. Microprobe analyses of newly formed minerals in the reaction zone

Component	Sub40		Sub41		Sub41		Sub41		Sub 111		Sub11 3		Sub11 3		Sub41	
	Cpx		*Opx* (Gls)		*Opx* (Hz)		*Phl*		*Omp*		*Opx* (Gls)		*Opx* (Hz)		*Chl* (Hz)	
	5*	sd	5	sd	4	sd	12	sd	8	sd	14	sd	6	sd	7	sd
SiO_2	55.90	0.55	56.44	2.26	56.3	0.71	42.81	1.03	54.99	0.98	55.28	0.56	54.50	0.64	31.87	1.44
TiO_2	0.27	0.13	0.08	0.09	0.03	0.04	0.42	0.23	0.26	0.06	0.07	0.04	0.06	0.02	0.05	0.06
Al_2O_3	9.41	1.17	1.79	0.64	0.89	0.17	10.84	1.31	10.81	0.92	2.74	0.35	3.13	0.57	14.01	0.79
Cr_2O_3	0.58	0.19	0.20	0.17	0.35	0.17	0.09	0.16	0.77	0.07	0.24	0.11	0.37	0.16	1.42	0.39
FeO	4.16	1.12	9.82	2.56	6.88	0.81	4.97	1.64	3.72	0.25	9.05	1.40	6.58	0.78	2.95	0.15
MnO	0.09	0.02	0.15	0.10	0.13	0.06	0.05	0.06	0.08	0.01	0.11	0.01	0.12	0.01	0.03	0.05
MgO	12.13	1.74	30.86	2.52	33.4	0.89	22.59	1.67	10.61	1.24	31.33	1.62	33.85	0.97	29.92	1.27
CaO	11.52	1.46	0.18	0.09	0.36	0.16	0.06	0.55	12.29	1.28	0.38	0.13	0.52	0.16	0.05	0.10
Na_2O	5.80	0.73	0.18	0.07	0.08	0.07	0.33	0.27	6.21	0.49	0.15	0.03	0.11	0.02	0.10	0.09
K_2O	0.02	0.02	0.34	0.44	0.05	0.08	6.78	1.04	0.04	0.05	0.28	0.26	0.13	0.12	0.05	0.03
NiO	–		–		–		–	1.99	0.03	0.01	0.16	0.04	0.14	0.04	–	
Total	99.88	0.75	100.05	2.69	98.5	1.84	88.94	0.04	99.79	0.52	99.63	0.88	99.37	0.99	80.45	3.22
X_{Mg}	0.84	0.05	0.85	0.04	0.90	0.01	0.89		0.83	0.02	0.86	0.02	0.90	0.01	0.95	0.01
X_{Ca}^{Grt}																
X_{Na}^{Bt}							0.07	0.07								
X_{Jd}^{Cpx}	0.36	0.05							0.36	0.06						

Abbreviations: *Opx*(Gls), grains near the glaucophane schist layer; *Opx*(Hz), grains near the harzburgite layer; *Chl*(Hz), grains within the harzburgite layer. "sd" is standard deviation. A dash indicates that the element was not analyzed. * Number of analyses.

crustal material into websterite, which could be related to the openness of the system or some specific features of high-pressure mineral formation in amphibolite.

Thus, the source of Ca and Mg interacting with glaucophane via reaction (1) is reactions (2) and (3) leading to the decomposition of the minerals of ultramafics.

The reaction zones have sharp boundaries (fronts) marked by the disappearance of a certain initial mineral and appearance of one or two new minerals (Fig. 2). The thinness of the reaction zones (~150–250 μm) and regular variations in the composition of newly formed minerals (orthopyroxene in the harzburgite layer and omphacite in the websterite layer) indicate that diffusion metasomatism occurred within them (Korzhinskii, 1982).

The zones of alteration along grain boundaries are much thicker than the reaction zones; they extend into the ultramafic layers above the reaction zones up to the upper lids of the capsules, which suggests that fluid infiltration dominated over diffusion during the experiments. In such a case, infiltration is related to a porous flow of fluid. A characteristic feature of this flow is extensive fluid (melt) interaction with the matrix (e.g., Grant et al., 2016; Perchuk et al., 2018), which results in significant compositional changes in both fluid and host rock (Manning, 2004).

Eclogitization of Glaucophane Schist

The transformation of glaucophane schist to eclogite can be observed in high-pressure complexes less frequently than, for instance, the eclogitization of amphibolites or gabbroids. The isochemical transformation of glaucophane schist to eclogite is often described by the reaction between glaucophane and clinozoisite:

$$Czo + Gln \rightarrow Omp + Grt + Qz + Par + H_2O,$$

which was demonstrated by the investigation of high-pressure rocks on the island of Syros, Greece (Ridley, 1984). The product of this reaction is the white mica paragonite, which does not always occur in eclogites formed after glaucophane schists in subduction complexes; this implies that the eclogitization of glaucophane schist may proceed via another path, including nonisochemical one. A spectacular example of such replacement was described in the Tien Shan high-

pressure belt (John et al., 2008), where the eclogite assemblage (*Omp* + *Grt* + *Phn*) develops in a system of veins in glaucophane schist consisting of more than 50% glaucophane. Our experiments also exemplify a nonisochemical replacement process.

In order to determine the possible mineral assemblage and estimate the probability of closed-system partial melting of the initial glaucophane schist under the *P–T* conditions of the experiments, we used the PerpleX program package (version 6.7.7) developed by Connolly (2005) for the construction of phase diagrams for a given chemical composition of the system using a thermodynamic data base for minerals and fluids. The chemical composition of schist was based on the XRF data (Table 1). Calculations were performed for systems with H_2O and H_2O–CO_2 fluids. Some simplifications were used in the calculations, but, in our opinion, they did not significantly affect the results. In particular, it was assumed that all Fe was present in the ferrous form, and Ti, Cr, and Mn oxides were ignored, because of their low contents and/or the absence of reliable thermodynamic data for respective solid solutions in minerals. An H_2O content of 3 wt % was assumed in accordance with the deviation of the totals of oxides in the schist analysis from 100 wt % (Table 1), if all Fe is calculated in the ferrous form. Modeling with mixed fluid was performed for 1.5 wt % H_2O and 1.5 wt % CO_2. The following solid solution models were used: Gt(HP) (as designated in the program) for garnet (Holland and Powell, 1998), Cpx(HP) and Opx(HP) for clinopyroxene and orthopyroxene (Holland and Powell, 1996), GlTrTsPg for amphibole (modified model of Powell and Holland, 1999), Mica(W) and Bi(W) for micas (White et al., 2014), and melt(W) for melt (White et al., 2014).

The thermodynamic modeling showed (Figs. 7a, 7b) that glaucophane schist with an initial H_2O content of 3 wt % must be replaced by the assemblage *Opx* + *Omp* + *Phn* + *Coe* coexisting with aqueous fluid under the experimental *P–T* conditions. At equal contents of H_2O and CO_2 (1.5 wt % each), magnesite is added to the assemblage (*Opx* + *Omp* + *Phn* + *Coe* + *Mst* + H_2O) under the same *P–T* conditions. The results of modeling are in good agreement with the presence of omphacite and SiO_2 in the experimental products. In the diagrams (Figs. 7a, 7b), the point of experimental conditions falls very near the stability field of garnet, the hydrous solidus, and the quartz–coesite transition; taking into account the uncertainty of thermodynamic modeling this is consistent with the presence of garnet and quartz in the newly formed assemblages and the absence of visible melt. The most important difference is that the model assemblages contain more than 1/3 orthopyroxene, which is at variance with the experiment. Even in the only experiment in which orthopyroxene growth was observed (Sub41), its content in the schist layer was no higher than 5 wt %, and it is mainly concentrated in the upper part of this layer owing to the input–output of components.

There are several possible reasons for the discrepancy between the results of modeling and experiments. First, the experimental products are almost devoid of initial winchite, epidote, and titanite, which are sources of Ca and Fe for the eclogite assemblage. Therefore, it can be expected that the assemblage and composition of minerals in a longer experiment will be shifted to some degree toward the model results. Second, the specific feature of metasomatic mineral formation accompanied by changes in protolith composition owing to the input–output of components and variations in their activities should be taken into account.

On the Fluid Phase and Character of CO_2 Migration in the Experiments

The experimental pressure was significantly lower than the second critical point in the basalt + H_2O system (e.g., Hermann et al., 2006). Consequently, the metasomatic transformations in the capsules could not be caused by a supercritical fluid, and the mobile phase was either H_2O–CO_2 fluid or silicate melt containing these volatile components. On the one hand, the possibility of partial melting of the schist is indicated by experimental data on eclogite melting in the presence of excess H_2O (Lambert and Wyllie, 1972): the temperature of our experiments is ~50°C higher than the hydrous solidus of eclogite. On the other hand, the chemical composition of the initial glaucophane schist is different from that of ordinary metabasite (for instance, MORB) in lower Al and Ca contents and higher contents of Si, Fe, Mg, and Na. Therefore, a direct comparison with the hydrous eclogite solidus (Lambert and Wyllie, 1972) is not strictly valid in this case. Moreover, the results of phase equilibrium modeling exclude any significant melting under the experimental *P–T* conditions (Fig. 7). Thus, H_2O–CO_2 fluid with dissolved components rather than melt was probably the main metasomatic agent. Note that the mantle materials could not undergo partial melting under the experimental *P–T* conditions, because the hydrous solidus of these rocks lies at higher temperatures (Kushiro, 1969; Parman and Grove, 2004; Safonov and Butvina, 2013).

Our modeling predicts that magnesite must be present in the glaucophane schist in the presence of CO_2 (Fig. 7b). However, significant magnesite growth in the schist layer was observed only in run Sub111 with the websterite mantle material, which is not favorable for carbonate growth under the experimental *P–T* conditions. A similar process occurred probably in run Sub40, but the small amount of CO_2 in the starting material could result in a negligible amount of newly formed carbonate in the experimental products. Note that the experiments with the harzburgite mate-

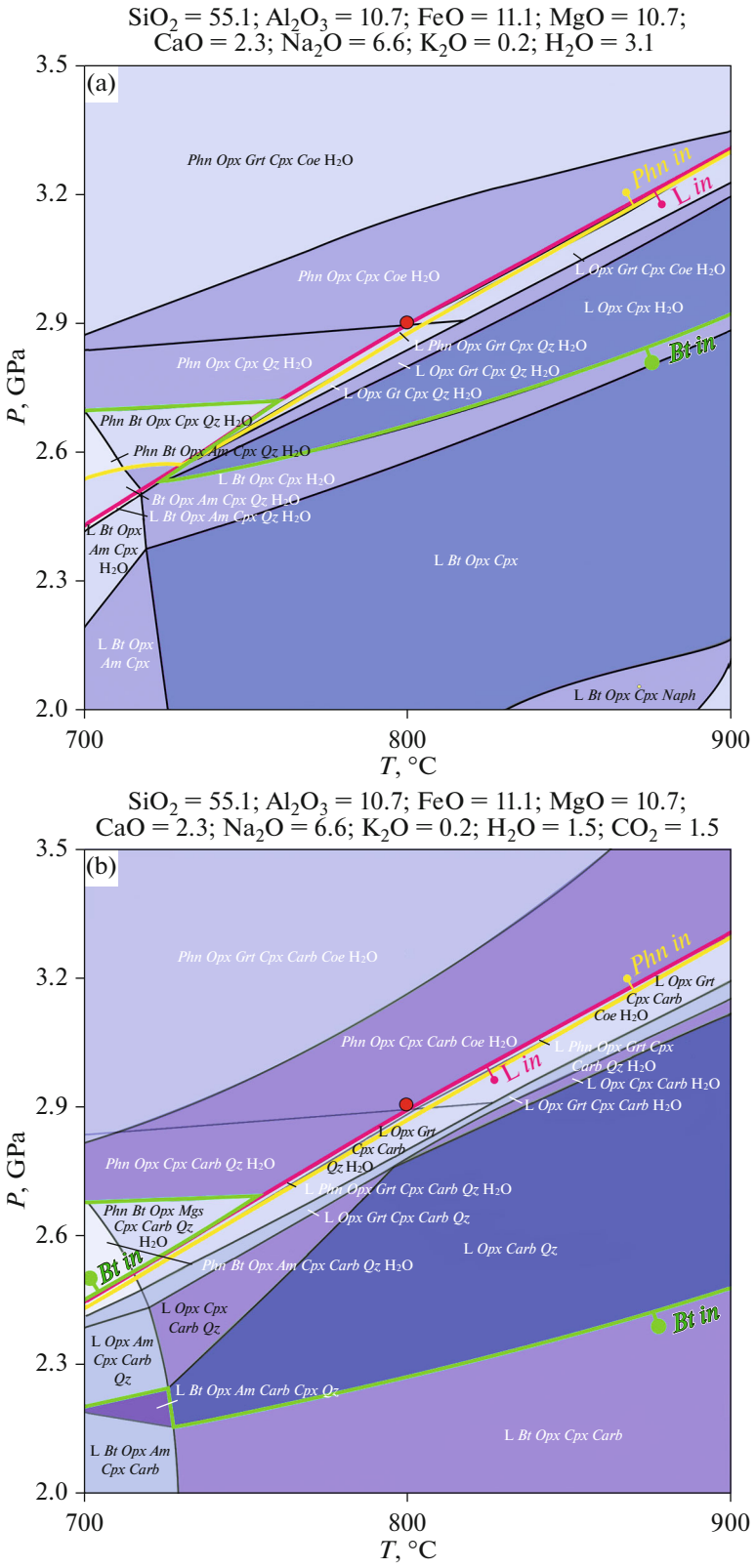

Fig. 7. Phase diagrams for the chemical composition of glaucophane schist obtained using the PerpleX program package (Connolly, 2005): (a) 3 wt % H_2O and (b) 1.5 wt % H_2O + 1.5 wt % CO_2. Mineral symbols are after Kretz (1983), and L is melt. See text for further explanation.

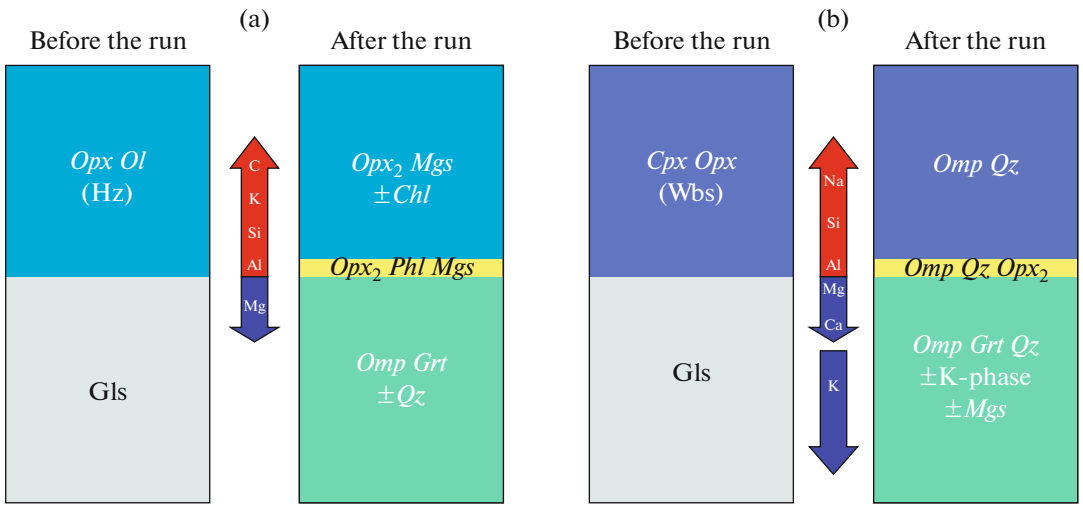

Fig. 8. Schematic presentation of processes in the capsules: (a) interaction in the Gls–Hz system, and (b) interaction in the Gls–Wbs system. Arrows indicate the direction of the mass transfer of components between layers and potassium in the schist layer.

rial confirmed the dissolution of initial calcite in the ascending flow of aqueous fluid, which was observed in previous experiments with dunitic and lherzolitic mantle layers (Perchuk and Korepanova, 2011; Perchuk et al., 2018). The new experimental series provided convincing evidence that CO_2 could play no significant role in the ascending flow of aqueous fluid, redepositing in the initial crustal material, if the mantle layer in the capsule is composed of websterite.

On the Perfectly Mobile Behavior of Components

Korzhinskii (1957, p. 178) noted that "the contents of inert components in metamorphic rocks correspond more or less to their content in the initial rock, whereas the contents of perfectly mobile components do not show such an inheritance and depend on the external conditions and inert-component composition". Based on this definition, it can be concluded that there is evidence for the perfectly mobile behavior, at least in the reaction zones, of Si, Al, Mg, K (in the apoharzburgite zone), Na, and Al (in the apowebsterite zone) and inert behavior of Fe and Ca. The driving force of mass transfer controlling the development of a metasomatic front is the gradient of chemical potential for most components resulting in the opposite fluxes of components through the boundary between the schist and ultramafic layers (Fig. 8). The existence of a gradient is not always necessary for the migration of K, Na, and CO_2 (Fig. 8); in such a case, the components were redeposited as newly formed minerals in their source layer.

Natural Analogues

It should be kept in mind that the spatiotemporal conditions and the diversity of magmatic and tectonometamorphic processes occurring in deep subduction environments cannot be reproduced in experimental setups. On the other hand, such processes cannot be directly observed, and laboratory experiments combined with the investigation of rocks from (ultra)high-pressure metamorphic complexes (Gilliot et al., 2009) and numerical geodynamic modeling (Gerya, 2011) play an important role in the reconstruction of the character of crust–mantle interaction and mass transfer, which is controlled to a large extent by deep fluids released from the subducting plate (Rapp et al., 1999; Pirard and Hermann, 2015a; Zheng et al., 2011; Spandler and Pirard, 2013; Schmidt and Poli, 2014; Woodland et al., 2018).

An important criterion for the testing of the feasibility of the experimental approach and the significance of experimental results is their verification on the basis of natural objects. It is shown below that the experimental results described above are in good agreement with natural observations.

The presence of phlogopite in mantle peridotites and pyroxenites is usually considered to be one of the most important indicators of deep modal metasomatism (O'Reilly and Griffin, 2013). Depending on *P–T* conditions, aqueous solution, melt, and supercritical fluid are possible metasomatic agents. These phases are practically not retained in mantle rocks, and the nature of the agent can be determined only indirectly from the products of metasomatic reactions (for instance, from the geochemistry of newly formed minerals). In the rocks of the subcratonic mantle, phlogopite usually grows together with clinopyroxene during fertilization under the influence of alkaline

melts (O'Reilly and Griffin, 2013, and reference therein). The development of metasomatic orthopyroxene (±*Grt*, ±*Mgs*) after olivine is more characteristic of the suprasubduction mantle (e.g., Malaspina et al., 2006); such assemblages we observed in our experiments on the interaction of carbonated amphibolite with dunite and lherzolite (Perchuk et al., 2018). The growth of metasomatic orthopyroxene and phlogopite was observed by Ertan and Leeman (1996) in mantle xenoliths from the volcanic rocks of the southern Cascade Mountains, United States. These authors suggested that the rocks underwent multistage metasomatism caused by high-K silicate melts and CO_2 fluid. Hence, our experiments reproduce a natural metasomatic process in the mantle wedge of the subduction zone beneath the Cascade Mountains, which is considered a classic example of a hot subduction zone (Syracuse et al., 2010). Potassic metasomatism and carbonation are controlled in this case to a large extent by the peridotite material of the mantle.

Because of the minor abundance of mantle websterites, the metasomatic alteration of these rocks is a much more local process compared with the metasomatism of dominant mantle peridotites. The probability of finding a metasomatized websterite is therefore not high. Some analogy with our experimental results can be supposed in a 3-cm xenolith of quartz websterite from the alkali basalt of western Hungary (Bali et al., 2008). Pyroxenes of these rocks contain silicic melt inclusions and show slab geochemical signatures (elevated contents of LILE and LREE and negative Nb, Ta, and Sr anomalies); they were interpreted by the authors as the result of metasomatic alteration of peridotite in the suprasubduction mantle. Taking into account the exotic occurrence of quartz-bearing websterite xenoliths, it can be suggested that the protolith could be represented in this case by rocks of the pyroxenite rather than peridotite suite.

Bimineralic omphacite–orthopyroxene and omphacite–quartz inclusions in diamond from kimberlite-borne mantle xenoliths deserve special attention (Sobolev et al., 1999). Their origin can now be considered not only in connection with an eclogite assemblage but also with metasomatically altered websterites.

CONCLUSIONS

The experiments described in this paper showed that the character of metasomatic processes and mass transfer at the crust–mantle boundary at sub-arc depths can be significantly affected by the suprasubduction mantle protolith. The most interesting observation is the spatial separation of alkaline components in an ascending fluid flow. The main source of these components was glaucophane schist; during eclogitization Na was transported from this material by aqueous fluid only into a websterite protolith, and K, only into a harzburgite protolith. With application to the subduction zone, this may indicate that the presence of peridotite material in the suprasubduction mantle favorable for K extraction from subducting metabasites, which prevents the formation of phengite in eclogites, the most important host for water at these depths (van Keken et al., 2011). The decomposition of this mineral is thought to cause dehydration melting in the slab and formation of silicic melts. In contrast, the presence of a websterite layer in the mantle is favorable for the preservation of K-mica in eclogite providing thus a reservoir of aqueous fluid and potential for partial melting at greater depth compared with the case of a metabasic layer overlain by harzburgitic mantle material. Note that, owing to the coupling of the subducting plate and suprasubduction mantle and their common downwelling, heterogeneities in the mineral and chemical compositions of the crustal and mantle rocks of the contact zone can be preserved to great depths. Potassium and structural water will descend either with crustal materials beneath altered websterite or at a higher structural level with the altered harzburgite layer.

The opposite fluxes of alkalis imply that the transport of large ion lithophile elements (LILE) and light rare earth elements (LREE) from the slab is dependent on the composition of mantle material, which will be reflected in the contents of these components in island-arc volcanic rocks.

Carbon transport also depends on the mantle protolith. Although the thermodynamic modeling indicated magnesite stability under the experimental P–T conditions (Fig. 7b), carbonate was not preserved in the metabasite in the presence of an overlying harzburgite layer, where carbonate was redeposited owing to dissolution and transport by the ascending fluid. The removal of carbonates from the rocks of subducting plates was described in high-pressure complexes (Frezzotti et al., 2011; Ague and Nicolescu, 2014) and experimentally reproduced by Perchuk and Korepanova (2011) and Perchuk et al. (2018). Our study showed that this process can be inhibited if the carbonated metabasite is overlain by websterite.

The possible occurrence of the established effects in natural environments suggests that the direct application of phase diagrams for the modeling of high-pressure processes in subduction zones or evaluation of H_2O and CO_2 budgets may be misleading.

ACKNOWLEDGMENTS

We are grateful to V.M. Polukeev (Institute of Experimental Mineralogy, Russian Academy of Sciences) for help in the experimental work, S.T. Podgornova for contribution to the preparation of the manuscript, E.N. Gramenitskii (Faculty of Geology, Moscow State University), O.G. Safonov (Institute of Experimental Mineralogy, Russian Academy of Sciences), E.M. Spiridonov, and B.B. Shkurskii (Faculty of Geology, Moscow State University) for the discus-

sion of our results. The constructive review of A.V. Girnis (Institute of Geology of Ore Deposits, Petrography, Mineralogy, and Geochemistry, Russian Academy of Sciences) helped to improve the manuscript. Equipment purchased with funds from the Program of the Development of the Moscow State University was used in our investigations. This study was financially supported by the Russian Foundation for Basic Research, project no. 16-05-00495.

REFERENCES

Ague, J.J. and Nicolescu, S., Carbon dioxide released from subduction zones by fluid-mediated reactions, *Nature Geosci.,* 2014, vol. 7, pp. 355–360.

Arai, S. and Ishimaru, S., Insights into petrological characteristics of the lithosphere of mantle wedge beneath arcs through peridotite xenoliths: a review, *J. Petrol.,* 2008, vol. 49, no. 4, pp. 665–695.

Bali, E., Zajacz, Z., Kovacs, I., et al., A quartz-bearing orthopyroxene-rich websterite xenolith from the Pannonian Basin, western Hungary: evidence for release of quartz-saturated melt from a subducted slab, *J. Petrol.,* 2008, vol. 49, pp. 421–439.

Bebout, G.E., Metamorphic chemical geodynamics of subduction zones, *Earth Planet. Sci. Lett.,* 2007, vol. 260, pp. 373–393.

Berly, T.J., Hermann, J., Arculus, R.J., and Lapierre, H., Supra-subduction zone pyroxenites from San Jorge and Santa Isabel (Solomon Islands), *J. Petrol.,* 2006, vol. 47, pp. 1531–1555.

Bose, K. and Ganguly, J., Quartz–coesite transition revisited: reversed experimental determination at 500–1200-degrees-C and retrieved thermochemical properties, *Am. Mineral.,* 1995, vol. 80, pp. 231–238.

Bulatov, V.K., Brey, G.P., Girnis, A.V., et al., Carbonated sediment–peridotite interaction and melting at 7.5–12 GPa, *Lithos,* 2014, vol. 200–201, pp. 368–385.

Cloos, M., Flow melanges: numerical modeling and geologic constraints on their origin in the Franciscan subduction complex, California, *Geol. Soc. Am. Bull.,* 1982, vol. 93, pp. 330–345.

Comodi, P., Nazzareni, S., Fumagalli, P., and Capitani, G.C., The peculiar crystal-chemistry of phlogopite from metasomatized peridotites: evidence from laboratory and nature, *Period. Mineral.,* 2011, vol. 80, pp. 181–197.

Connolly, J.A.D., Computation of phase equilibria by linear programming: a tool for geodynamic modeling and its application to subduction zone decarbonation, *Earth Planet. Sci. Lett.,* 2005, vol. 236, pp. 524–541.

Ertan, I.E. and Leeman, W.P., Metasomatism of Cascades subarc mantle: evidence from a rare phlogopite orthopyroxenite xenolith, *Geology,* 1996, vol. 24, pp. 451–454.

Frezzotti, M.L., Selverstone, J., Sharp, Z.D., and Compagnoni, R., Carbonate dissolution during subduction revealed by diamond-bearing rocks from the Alps, *Nature Geosci.,* 2011, vol. 4, pp. 703–706.

Gervasoni, F., Klemme, S., Rohrbach, A., et al., Experimental constraints on mantle metasomatism caused by silicate and carbonate melts, *Lithos,* 2017, vol. 282–283, pp. 173–186.

Gerya, T., Future directions in subduction modeling, *J. Geodynamics,* 2011, vol. 52, pp. 344–378.

Gerya, T.V., Stoeckhert, B., and Perchuk, A.L., Exhumation of high-pressure metamorphic rocks in a subduction channel: a numerical simulation, Tectonics, 2002, vol. 21, no. 6, doi 10.1029/2002TC001406

Grant, T., Harlov, D.E., and Rhede, D., Experimental formation of pyroxenite veins by reactions between olivine and Si, Al, Ca, Na, and Cl-rich fluids at 800°C and 800 MPa: implications for fluid metasomatism in the mantle wedge, *Am. Mineral.,* 2016, vol. 101, pp. 808–818.

Guillot, S., Hattori, K., Agard, P., et al., *Exhumation processes in oceanic and continental subduction contexts: a review, Subduction Zone Geodynamics,* Lallemand, S. and Funiciello, F., Eds., Heidelberg and Berlin: Springer, 2009.

Hermann, J., Spandler, C., Hack, A., and Korsakov, A.V., Aqueous fluids and hydrous melts in high-pressure and ultra-high pressure rocks: implications for element transfer in subduction zones, *Lithos,* 2006, vol. 92, pp. 399–417.

Holland, T. and Powell, R., Thermodynamics of order–disorder in minerals. 2. Symmetric formalism applied to solid solutions, *Am. Mineral.,* 1996, vol. 81, pp. 1425–1437.

Holland, T.J.B. and Powell, R., An internally consistent thermodynamic data set for phases of petrological interest, *J. Metamorph. Geol.,* 1998, vol. 16, pp. 309–343.

John, T., Klemd, R., Gao, J., and Garbe-Schonberg, C.D., Trace-element mobilization in slabs due to non steady-state fluid–rock interaction: constraints from an eclogite-facies transport vein in blueschist (Tianshan, China), *Lithos,* 2008, vol. 103, pp. 1–24.

Kepezhinskas, P.K., Defant, M.J., and Drummond, M.S., Na metasomatism in the island-arc mantle by slab–peridotite interaction: evidence from mantle xenoliths in the north Kamchatka arc, *J. Petrol.,* 1995, vol. 36, pp. 1505–1527.

Khodorevskaya, L.I. and Zharikov, V.A., Experimental simulation of amphibolite and ultrabasic rock interaction in subduction zones, *Petrology,* 1997, vol. 5, pp. 2–8.

Korzhinskii, D.S., *Fiziko-khimicheskie osnovy analiza parageneziso mineralov* (Physicochemical Basis of the Analysis of Mineral Parageneses), Moscow: AN SSSR, 1957.

Korzhinskii, D.S., *Teoriya metasomaticheskoi zonal'nosti* (Theory of Metasomatic Zoning), Moscow: Nauka, 1982.

Kretz, R., Symbols for rock-forming mineral, *Am. Mineral.,* 1983, vol. 68, pp. 277–279.

Krogh Ravna, E. J., The garnet–clinopyroxene Fe^{2+}–Mg geothermometer: an updated calibration, *J. Metamorph. Geol.,* 2000, vol. 18, pp. 211–219.

Kushiro, I., The system forsterite–diopside–silica with and without water at high pressures, *Am. J. Sci.,* 1969, vol. 267A, pp. 269–294.

Lambert, I.B. and Wyllie, P.J., Melting of gabbro (quartz eclogite) with excess water to 35 kilobars, with geological applications, *J. Geol.,* 1972, vol. 80, pp. 693–708.

Malaspina, N., Hermann, J., Scambelluri, M., and Compagnoni, R., Polyphase inclusions in garnet-orthopyroxenites (debie shan, china) as monitors for metasomatism and fluid-related trace element transfer in subduction zone peridotite, *Earth Planet. Sci. Lett.,* 2006, vol. 249, pp. 173–187.

Manning, C.E., The chemistry of subduction-zone fluids, *Earth Planet. Sci. Lett.,* 2004, vol. 223, pp. 1–16.

O'Reilly, S.Y. and Griffin, W.L., Mantle metasomatism, *Metasomatism and the Chemical Transformation of Rock,* Harlov, D.E. and Austrheim, H., Eds., *Lecture Notes Earth Syst. Sci.,* Berlin and Heidelberg: Springer, 2013.

Parman, S.W. and Grove, T.L., Harzburgite melting with and without H_2O: experimental data and predictive modeling, *J. Geophys. Res.,* 2004, vol. 109, B02201, doi 10.1029/2003JB002566

Patiño Douce, A.E. and Harris, N., Experimental constraints on Himalayan anatexis, *J. Petrol.,* 1998, vol. 39, pp. 689–710.

Perchuk, A.L. and Korepanova, O.S., The problem of CO_2 recycling in subduction zones, *Mosk. Univ. Geol. Bull.*, 2011, vol. 66, no. 4, pp. 250–260.

Perchuk, A.L. and Yapaskurt, V.O., Experimental simulation of orthopyroxene enrichment and carbonation in the suprasubduction mantle under the influence of H_2O, CO_2, and SiO_2, *Geochem. Int.,* 2013, vol. 51, no. 4, pp. 257–268.

Perchuk, A.L., Shur, M.Yu., Yapaskurt, V.O., and Podgornova, S.T., Experimental modeling of mantle metasomatism coupled with eclogitization of crustal material in a subduction zone, *Petrology,* 2013, vol. 21, no. 6, pp. 579–598.

Perchuk, A.L., Yapaskurt, V.O., Griffin, W.G., et al., Three types of element fluxes from metabasite into peridotite in analogue experiments: insights into subduction-zone processes, *Lithos,* 2018, vol. 302–303, pp. 203–223.

Pirard, C. and Hermann, J., Focused fluid transfer through the mantle above subduction zones, *Geology,* 2015a, vol. 43, pp. 915–918.

Pirard, C. and Hermann, J., Experimentally determined stability of alkali amphibole in metasomatised dunite at sub-arc pressures, *Contrib. Mineral. Petrol.,* 2015b, vol. 169, no. 1, pp. 1–26.

Powell, R. and Holland, T., Relating formulations of the thermodynamics of mineral solid solutions: activity modeling of pyroxenes, amphiboles, and micas, *Am. Mineral.,* 1999, vol. 84, pp. 1–14.

Rapp, R.P., Shimizu, N., and Norman, M.D., Reaction between slab-derived melts and peridotite in the mantle wedge: experimental constraints at 3.8 GPa, *Chem. Geol.,* 1999, vol. 160, pp. 335–356.

Ridley, J., Evidence of a temperature-dependent 'blueschist' to 'eclogite' transformation in high-pressure metamorphism of metabasic rocks, *J. Petrol.,* 1984, vol. 25, pp. 852–870.

Safonov, O.G. and Butvina, V.G., Interaction of model peridotite with H_2O–KCl fluid: experiment at 1.9 GPa and its implications for upper mantle metasomatism, *Petrology,* 2013, vol. 21, no. 6, pp. 599–615.

Scambelluri, M. and Philippot, P., Deep fluids in subduction zones, *Lithos,* 2001, vol. 55, pp. 213–227.

Schmidt, M.W. and Poli, S., *Devolatilization during subduction, Treatise on Geochemistry,* Holland H.D., and Turekian K.K., Eds., 2014, pp. 669–701.

Sekine, T. and Wyllie, P.J., The system granite–peridotite–H_2O at 30 kbar, with applications to hybridization in subduction zone magmatism, *Contrib. Mineral. Petrol.,* 1982, vol. 81, pp. 190–202.

Sobolev, N.V., Sobolev, V.N., Snyder, G.A., et al., Significance of eclogitic and related parageneses of natural diamonds, *Int. Geol. Rev.,* 1999, vol. 41, pp. 129–140.

Spandler, C. and Pirard, C., Element recycling from subducting slabs to arc crust: a review, *Lithos,* 2013, vol. 170–171, pp. 208–223.

Syracuse, E.M., van Keken, P.E., and Abers, G.A., The global range of subduction zone thermal models, *Phys. Earth Planet. Inter.,* 2010, vol. 183, no. 1, pp. 73–90.

van Keken, P.E., Hacker, B.R., Syracuse, E.M., and Abers, G.A., Subduction factory: 4. Depth-dependent flux of H_2O from subducting slabs worldwide, *J. Geophys. Res.,* 2011, vol. 116, B01401, http://dx.doi.org/. doi 10.1029/2010JB007922

White, R.W., Powell, R., Holland, T.J.B., et al., New mineral activity–composition relations for thermodynamic calculations in metapelitic systems, *J. Metamorph. Geol.,* 2014, vol. 32, pp. 261–286.

Woodland, A.B., Bulatov, V.K., Brey, G.P., et al., Subduction factory in an ampoule: experiments on sediment–peridotite interaction under temperature gradient conditions, *Geochim. Cosmochim. Acta,* 2018, vol. 223, pp. 319–349.

Zheng, Y.F., Chen, R.X., Xu, Z., and Zhang, S.B., The transport of water in subduction zones, *Sci. China Earth Sci.,* 2016, vol. 59, pp. 651–682.

Translated by A. Girnis